



HAL
open science

Synthesis, crystallographic structure and thermodynamic properties of T₂-Al₂MgC₂

Guillaume Deffrennes, Bruno Gardiola, Erwann Jeanneau, Georges Mikaelian, Benigni P., Alain Pasturel, Alexander Pisch, J. Andrieux, Olivier Dezellus

► **To cite this version:**

Guillaume Deffrennes, Bruno Gardiola, Erwann Jeanneau, Georges Mikaelian, Benigni P., et al.. Synthesis, crystallographic structure and thermodynamic properties of T₂-Al₂MgC₂. *Journal of Solid State Chemistry*, 2019, 273, pp.150-157. 10.1016/j.jssc.2019.02.039 . hal-02062499

HAL Id: hal-02062499

<https://hal.science/hal-02062499v1>

Submitted on 2 Dec 2020

HAL is a multi-disciplinary open access archive for the deposit and dissemination of scientific research documents, whether they are published or not. The documents may come from teaching and research institutions in France or abroad, or from public or private research centers.

L'archive ouverte pluridisciplinaire **HAL**, est destinée au dépôt et à la diffusion de documents scientifiques de niveau recherche, publiés ou non, émanant des établissements d'enseignement et de recherche français ou étrangers, des laboratoires publics ou privés.

Synthesis, crystallographic structure and thermodynamic properties of T2-Al₂MgC₂

*Guillaume DEFFRENNES^a, Bruno GARDIOLA^a, Erwann JEANNEAU^b, Georges Mikaelian^c,
Pierre Benigni^c, Alain PASTUREL^d, Alexander PISCH^d, Jérôme ANDRIEUX^a, Olivier
DEZELLUS^{a*}*

a Laboratoire des Multimatériaux et Interfaces, Université Claude Bernard Lyon 1, Villeurbanne,
France

b Centre de Diffractométrie Henri Longchambon, Université Claude Bernard Lyon 1,
Villeurbanne, France

c Institut Matériaux Microélectronique Nanosciences de Provence, Universités d'Aix-Marseille et
de Toulon, Marseille, France

d Laboratoire de Science et Ingénierie des Matériaux et Procédés, Université Grenoble Alpes,
CNRS, Grenoble INP, Grenoble, France

Corresponding author : Dr. Olivier DEZELLUS

e-mail : olivier.dezellus@univ-lyon1.fr

Keywords : T2-Al₂MgC₂; Al-C-Mg; Crystal structure; Density Functional Theory (DFT);
Thermodynamic properties; Electronic structure; Phonons

Abstract

T2-Al₂MgC₂ was synthesized from the elements in a Mg-Al melt at 1000°C using sealed Ta crucibles. Single crystals of T2-Al₂MgC₂ were extracted by evaporating the Mg-Al matrix. The crystal structure of T2-Al₂MgC₂ was refined for the first time on the basis of single-crystal X-ray diffraction. The crystal is trigonal (space group P-3m1, Z=1) with lattice parameters of $a=3.3767(11)$ Å, $c=5.807(2)$ Å and $V=57.34(5)$ Å³. Based on the refined crystal structure, DFT calculations were conducted to evaluate the thermodynamic properties and the electronic structure of the phase. The heat of formation of T2-Al₂MgC₂ was calculated to be -23.6 kJ/moles of atoms at 298K. The heat capacity of T2-Al₂MgC₂ was measured by DSC from 300 to 871K and calculated by DFT from 0 to 1000K. Based on the calculated heat capacity, the entropy of formation of the phase at 298K was determined to be 70.0 J/mol/K. The band structure and the electronic density of state of T2-Al₂MgC₂ was calculated leading to an indirect band gap value of 1.73 eV.

1. Introduction

Refinement of the microstructure of Mg-based materials provides an avenue for promoting their competitiveness. As a matter of fact, a fine grain size leads to an improvement in creep resistance [1], ductility and strength [2–5], as well as corrosion resistance [6] of Mg alloys. Carbon inoculation is the primary method to achieve refined microstructures for Mg-Al alloys [7] while the underlying mechanisms remain uncertain. Recently strong evidence [4,8,9] pointed towards the heterogeneous nucleation of primary Mg on top of the Al_2MgC_2 ternary phase.

Another interesting approach for synthesizing mechanically-enhanced materials is the development of magnesium-based composites. Indeed, reinforcements may improve the creep resistance, strength and stiffness of the alloys. Various reinforcements were used to tailor the Mg-matrix composites properties, and in particular a variety of carbon-based reinforcements such as silicon carbide, titanium carbide, carbon nanotubes and boron carbide [10]. The formation of Al_2MgC_2 carbide at the fibre/matrix interfaces of a C/Mg-Al MMC has a considerable influence on the mechanical properties of the composite by changing the fibre/matrix bonding strength [11].

Although Al_2MgC_2 plays a major role in the grain refinement of Mg-Al alloys as well as in the mechanical properties of Mg-Al based composites, the ternary phase and its thermodynamic properties are not included in commercial thermodynamic databases [12–14]. This absence is due to the fact that the thermodynamic properties of Al_2MgC_2 are mostly unknown as the high vapour pressure and reactivity of Mg together with the fact that Al_2MgC_2 reacts vigorously with water [8,15] make experimental work difficult.

As the synthesis, extraction and handling of hygroscopic Al_2MgC_2 single-crystals is challenging, the crystal structure of this ternary carbide has only been determined by means of powder diffraction in past studies [15–17]. The crystal structure of T2- Al_2MgC_2 , the allotropic form of

Al_2MgC_2 which is stable above 727°C [16], was determined by Rietveld refinement by Bosselet et al. (Trigonal, P-3m1, $a=3.3770(9)$ Å, $c=5.817(1)$ Å) [16] and by Kubus and Meyer (Trigonal, P-3m1, $a=3.3676(1)$ Å, $c=5.7997(2)$ Å) [17]. The so-called T1- Al_2MgC_2 allotropic form of Al_2MgC_2 was found to be predominant below 717°C but could not be synthesized free of the T2 crystalline variety [16]. T1- Al_2MgC_2 was indexed with a hexagonal symmetry with $a=3.4017(7)$ Å and $c=12.292(2)$ Å [15]. While structural characterization by powder diffraction can be more practical than single-crystal diffraction techniques, the quality of the structural information obtained by the latter is considered to be more accurate and precise than the former [18].

A well-established crystal structure is a prerequisite in order to be able to perform predictive DFT (density functional theory) calculations. The heat of formation of the T2- Al_2MgC_2 carbide was calculated in the past using the GGA functional. The reported value with respect to Al-fcc, Mg-hcp and C-graphite is -0.064 eV/moles of atoms [19], i.e. -6.18 kJ/moles of atoms. Recently the authors investigated the heat of formation of Al_4C_3 in a study that will be published elsewhere [20]. It was shown that the heat of formation of this binary carbide calculated using the GGA functional was significantly too positive as compared to available experimental information, notably due to a large error in the ground state energy of C-graphite. This discrepancy can be explained by the fact that graphite, Al_4C_3 [21] and T2- Al_2MgC_2 are layered structures and that the GGA functional is not suited to describe the weak interactions in the bonding energy between the layers. Recently, the new SCAN (Strongly Conditioned and Appropriately Normed) semi-local density functional was introduced which is particularly suited to describe the ground state properties of layered materials [36]. As the SCAN functional gave much better results for Al_4C_3 and graphite [20] it was selected for this work on T2- Al_2MgC_2 .

In the present study, an alternative procedure to synthesize the T2-Al₂MgC₂ phase in a Mg-Al melt at 1000°C using sealed Ta crucibles was developed. Single-crystals of the carbide phase were obtained for the first time by evaporating the Mg-Al matrix at 800°C. The crystal structure of the T2-Al₂MgC₂ phase was confirmed from single-crystal X-ray diffraction and heat capacity measurements were performed by Differential Scanning Calorimetry (DSC). DFT calculations using the SCAN functional were conducted from the refined structure to determine the thermodynamic properties of the carbide phase.

2. Materials and methods

2.1. Materials

Commercial powders of magnesium (purity > 99,8 wt.%, grain size 150 < d < 850 µm, Alfa Aesar), aluminium (purity > 99,8 wt.%, grain size 44 < d < 420 µm, Alfa Aesar) and graphite (synthetic, d < 20 µm, Sigma Aldrich) were used in this study. The magnesium powder was selected to be coarse in order to reduce the surface/volume ratio and the amount of MgO impurities. The graphite powder was selected to be fine enough in order to avoid the isolation of coarse graphite particles from the melt by the formation of a carbide layer at the graphite/alloy interface.

2.2. Sample preparation

The powders were mixed in mass ratio of Mg : Al : C = 70 : 19 : 11 which was selected on the basis of the isothermal section proposed by Viala et al. at 727°C [15]. A liquid-rich overall composition is expected in order to ensure that the sample is homogeneous and to enable crystal growth. The selected overall composition is expected to lead to a three-phase equilibrium between T2-Al₂MgC₂, graphite and a magnesium-rich liquid with phase amounts being roughly 67 wt.% of Mg-rich matrix, 29wt.% of Al₂MgC₂ and 4wt.% of graphite. First of all, this ensured that the formation of Al₄C₃ was avoided. Secondly, with the perspective of extracting T2-Al₂MgC₂ single-

crystals by evaporating the matrix, a magnesium-rich matrix was desired as aluminium is less volatile than magnesium. Having a small amount of graphite as a side product ensures this requirement and increases the T2-Al₂MgC₂ yield.

The details of the sample preparation were given elsewhere [22]. The main steps are ball-milling of the powders in a tungsten carbide mortar and cold-pressing of the mixture under 250 MPa, both being performed under protective Ar atmosphere (H₂O = 26 ppm). Typical powder compacts weighed 80 mg. Tantalum crucibles (purity > 99,95wt.%, Concept Metal) sealed under an absolute pressure of 0.6 bar of Ar (purity > 99.9999 %, Alphagaz 2, Air Liquide) were used for the synthesis.

2.3. Synthesis of T2-Al₂MgC₂

The powder compacts placed in sealed Ta crucibles were heat treated at 1000±4°C for 240 hours. The Ta crucibles were sealed inside vitreous silica containers under an absolute Ar pressure of 0.2 bar in order to avoid external oxidation and oxygen diffusion through the Ta crucibles during the heat treatment. The initial sample composition was not altered by magnesium evaporation as only a negligible fraction of Mg was needed to supply its equilibrium vapour pressure given the crucibles volume [22]. The samples were efficiently quenched by breaking the silica containers as soon as they were removed from the furnace. X-ray diffraction was performed on the samples and the diffraction pattern is presented in Fig. 1.

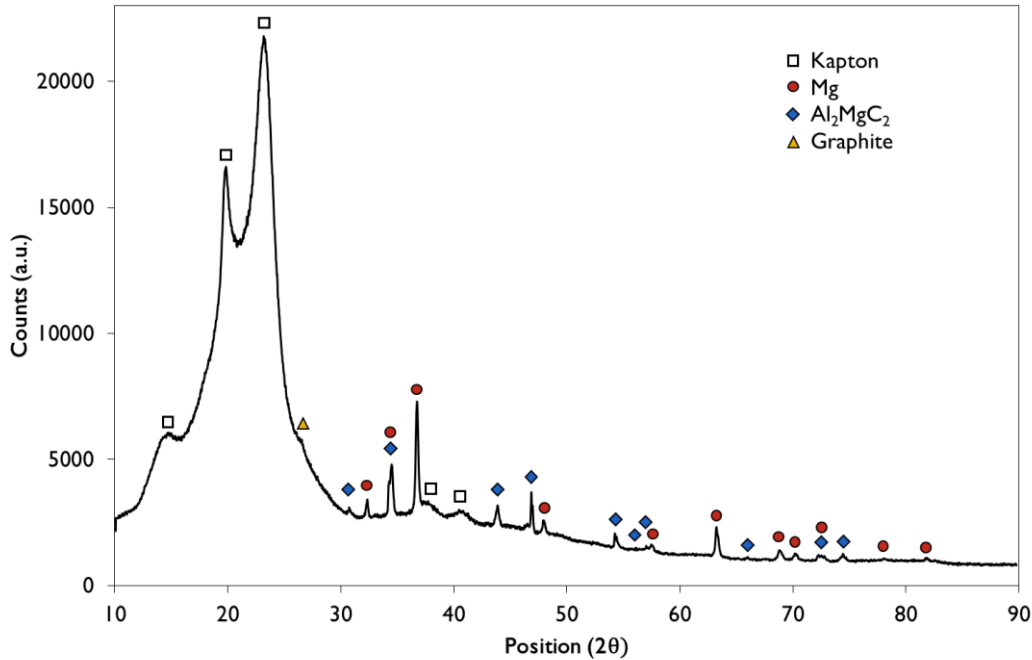


Figure 1. XRD Diffraction pattern of a 70Mg – 19Al – 11C sample heat-treated 240 hours at 1000°C and quenched. A kapton tape was used to protect Al₂MgC₂ from hydrolysis. The peaks attributed to Mg were shifted to account for the Al solid solution. No MgO could be detected within the detection range.

2.4 SEM-EDS

At the end of the heat treatments the Ta crucibles were opened using a diamond wire saw without adding any lubricant. Samples were embedded in resin and polished using a water-free procedure to prevent the hydrolysis of T2-Al₂MgC₂. The samples were pumped under dynamic high vacuum for a few hours to remove trapped solvent or gases from the porosities. A conductive silver paint was applied to the entire surface of the resin in air as quickly as possible ($t < 15$ min). The samples were again placed under dynamic high vacuum before being transported to the electron microscope in a static vacuum chamber. Standards made of Mg (purity > 99.9%, Goodfellow), Al (Purity > 99.999%, Alfa Aesar) and graphite (purity > 99.9958%, SIGRADUR[®] glassy carbon HTW) were

prepared following the same procedure. SEM observations were made on a Zeiss Merlin Compact SEM equipped with plasma cleaning equipment and an energy dispersive spectrometer (EDS). Plasma cleaning of the samples significantly reduced the oxygen content and the carbon contamination at the sample surface. An accelerating voltage of 10kV and a working distance of 8.5 mm were selected. For the EDS analysis, the beam was calibrated in energy using the graphite standard. A counting time of 20 seconds was used for the measurements. The concentration of each element was calculated from the ratios between intensity in the specimen and in the standard using the PAP model [23].

2.5 Extraction of T2-Al₂MgC₂

As no selective etching solution exists to dissolve an Mg-Al matrix from T2-Al₂MgC₂ crystals, the ternary carbide phase was extracted by evaporation of the Mg-Al matrix. After synthesis of T2-Al₂MgC₂ (cf. 2.2) the Ta crucibles were opened and placed inside a 304L stainless steel tube. The assembly was heated at 800±5°C in a conventional horizontal tube furnace with an Eurotherm controller under dynamic high vacuum. During the evaporation, the Mg vapours were trapped out of the furnace using a water-cooling circuit. After 30 minutes, the assembly was cooled in air before being opened under a protective Ar atmosphere.

2.6 Single-crystal X-ray diffraction

After the extraction of T2-Al₂MgC₂, the resulting mixture was plunged in a perfluoropolyether oil (FOMBLIN[®] YR1800, Solvay) to protect the T2-Al₂MgC₂ single-crystals from hydrolysis. A suitable crystal of T2-Al₂MgC₂ was selected and mounted on a Gemini kappa-geometry diffractometer (Rigaku OD, 2015) equipped with an Atlas CCD detector and using Mo radiation ($\lambda = 0.71073 \text{ \AA}$).

Intensities were collected at 150 K by means of the CrysAlisPro software [24]. Reflection indexing, unit-cell parameter refinement, Lorentz-polarization correction, peak integration and background determination were carried out with the CrysAlisPro software [24]. An analytical absorption correction was applied using the modelled faces of the crystal [25]. The resulting set of hkl was used for structure solution and refinement. The structures were solved by direct methods with SIR97 [26] and the least-square refinement on F^2 was achieved using the CRYSTALS software [27]. All atoms were refined anisotropically.

2.7 Differential Scanning Calorimetry

The heat capacity measurements were performed in a DSC 111 calorimeter from the Setaram Company by the so-called "small temperature steps procedure" or "discontinuous method" using the classical three steps method as described by Höhne et al. [28]. Extensive details on the experimental apparatus and protocol can be found elsewhere [29]. After the extraction of T2- Al_2MgC_2 , the resulting mixture was sealed in a stainless steel crucible under argon protective atmosphere ($\text{O}_2 < 1$ ppm, $\text{H}_2\text{O} = 26$ ppm) inside a glovebox. In total, four stainless steel crucibles were used. The first one was filled with 64.610 mg of the mixture resulting for the extraction of T2- Al_2MgC_2 , the second one with 61.375 mg of Standard Reference Material 720 $\alpha\text{-Al}_2\text{O}_3$ [30], and the third and fourth ones were sealed empty. The temperature program and the processing of the recorded thermograms were performed with the SETSOFT 2000 software provided by Setaram. A 2.5 K temperature step with a 1.5 K/min heating rate between each step and an 800 s stabilization time after each step were selected. The heat capacity measurements were performed between 300 and 871 K. A point by point correction factor, calculated from the ratio between the reference [30] and the apparent heat capacity of $\alpha\text{-Al}_2\text{O}_3$, was applied. Finally, it is important to note that the measurements are not performed on pure T2- Al_2MgC_2 but on the mixture resulting

from its extraction. Therefore corrections were applied for the impurities assuming that heat capacity were additive. The heat capacity function of the impurities used for the corrections were obtained from the NIST-JANAF thermochemical tables [31] and practical details are given in the discussion Section 3.3.

2.8 DFT calculations

The ground state properties of T2-Al₂MgC₂ were determined using DFT [32,33]. The VASP software package [34,35] in its most recent version (5.4.4) was used for the calculations.

The many-body exchange correlation functionals for the elements were selected using prior work by Pisch et al. on the ground state properties of Al₄C₃ [21]. For layered carbides, such as graphite, Al₄C₃ and Al₂MgC₂ in this contribution, the Strongly Conditioned and Appropriately Normed (SCAN) semi-local density functional [36] is particularly adapted. In addition, van der Waals interactions were added in the calculations to take into account the long-range order phenomena in these materials. The numerical routines from Klimes et al. [37,38] as implemented in the VASP code were used. For Al, the 3s and 3p orbitals, for C, 2p and 2s orbitals and for Mg the 3s orbitals are considered as valence states in the calculations. The energy cutoff for the projector augmented plane-wave bases was set to 800 eV. An automatically generated, gamma centered grid of k-points (26x26x15) in the irreducible part of the Brillouin zone was used following the Monkhorst-Pack scheme [39].

The lattice parameters of T2-Al₂MgC₂ as well as the internal atomic coordinates were fully relaxed. The linear tetrahedron method with Blöchl corrections [40] was used to calculate the electronic density of states (DOS). The relaxations were performed with a convergence criterion of 10⁻⁸ eV/Å for the total energy. The electronic band gap was calculated in the fully relaxed state.

Finite temperature properties such as Zero Point Energy (ZPE) or heat capacities at constant volume / pressure can be approximated using lattice dynamics theory. The phonon spectrum of Al_2MgC_2 was determined using the frozen-phonon (Supercell) method with a $3 \times 3 \times 2$ Supercell. The vibrational modes were calculated using the phonopy code [41] coupled to VASP. The convergence criterion for the Hellman-Feynman forces was set to 10^{-6} eV/Å to avoid any residual strain in the lattice.

The total energy of formation for T2- Al_2MgC_2 at 0K in kJ/mol is obtained by subtracting the weighted sum of the constitutive elements from the calculated ground state energy of the ternary compound:

$$\Delta H(\text{T2-Al}_2\text{MgC}_2) = E(\text{T2-Al}_2\text{MgC}_2) - (2 E(\text{Al-fcc}) + E(\text{Mg-hcp}) + 2 E(\text{C-graphite}))$$

This formation energy is then corrected with respect to the calculated ZPE energies:

$$\Delta H^{\text{cor}}(\text{T2-Al}_2\text{MgC}_2) = \Delta H(\text{T2-Al}_2\text{MgC}_2) + \Delta \text{ZPE}(\text{Al}_2\text{MgC}_2)$$

for which the ZPE correction was calculated as follows:

$$\Delta \text{ZPE}(\text{T2-Al}_2\text{MgC}_2) = \text{ZPE}(\text{T2-Al}_2\text{MgC}_2) - (2 \text{ZPE}(\text{Al-fcc}) + \text{ZPE}(\text{Mg-hcp}) + 2 \text{ZPE}(\text{C-graphite}))$$

The heat capacity at constant volume can be calculated in the harmonic approximation (HA) using the phonon density of states as a function of frequency q of the band s :

$$F(V_0, T) = \frac{1}{2} \sum_{q,s} \hbar \omega(q, s) + k_B T \sum_{q,s} \ln \left[1 - \exp \left(\frac{-\hbar \omega(q,s)}{k_B T} \right) \right]$$

The vibrational entropy and the heat capacity at constant volume are given by:

$$S = - \left(\frac{\partial F}{\partial T} \right)_V ; C_V = -T \left(\frac{\partial^2 F}{\partial T^2} \right)_V$$

When repeating the HA calculations for several different volumes V to obtain a minimum value of $F(V, T)$, the heat capacity at constant pressure in the quasi-harmonic approximation QHA can be calculated using:

$$C_p = -T \left(\frac{\partial^2 G(T, P)}{\partial T^2} \right)$$

with $G(T, P) = \min_V [E(V) + F(V; T) + PV]$.

The standard heat of formation at 298K of T2-Al₂MgC₂ was calculated using the calculated C_p value from the quasi-harmonic approximation and the heat content values for the pure elements Al-fcc, Mg-hcp and C-graphite from NIST-JANAF [31]. In addition, using the calculated thermal expansion coefficient, the volume evolution can be calculated as a function of temperature. The calculated cell volume value at 150K was compared to the experimental value.

3. Results and discussion

3.1 Synthesis of T2-Al₂MgC₂

The T2-Al₂MgC₂ carbide was synthesized at 1000±4°C for 240 hours from the composition 70Mg – 19Al – 11C wt.%. As expected from the isothermal section proposed by Viala et al. [15], stoichiometric T2-Al₂MgC₂ crystals were obtained in a 97.7Mg-2.3Al wt.% (97.9Mg-2.1Al at.%) matrix along with graphite located at the carbide – matrix interface and a few MgO particles. This microstructure is shown in Fig. 2. Al₂MgC₂ crystals were hexagonal and rectangular shaped. The MgO particles can be differentiated from the T2-Al₂MgC₂ crystals as they appear darker, have softer edges, and are smaller. The results of the phase characterization by EDS measurements are displayed in Table 1. The Al₂MgC₂ composition was determined statistically from a set of 19 crystals and is given for each element with an expanded uncertainty with 0.95 level of confidence. The results are in good agreement with the theoretical phase stoichiometry. No carbon could be detected in solution in the Mg-Al matrix within the detection limit. The limited amount of aluminium found in the matrix after the syntheses is an evidence that thermodynamic equilibrium was reached. Moreover, the Al content of 2.3 wt.% (2.1 at.%) in the matrix which was in equilibrium with both graphite and T2-Al₂MgC₂ at 1000°C is consistent with the value of 0.6

wt.%Al measured after syntheses at 727°C by Viala et al. [15]. However, it is worth noting that this composition is obtained after quenching the samples in the present study, and after natural cooling in the case of Viala et al. [15].

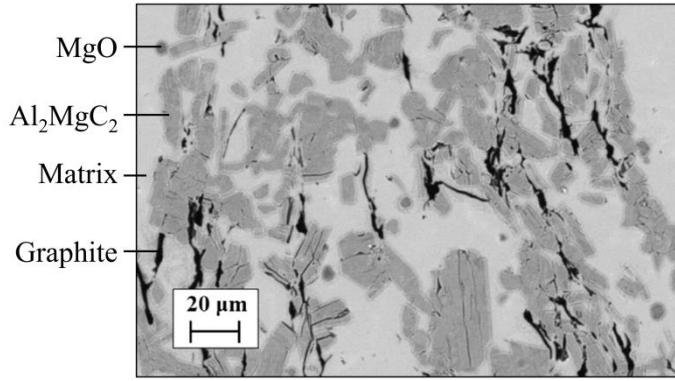


Figure 2. SEM observation of a 70Mg – 19Al – 11C sample heat-treated 240 hours at 1000°C. The microstructure is characterized by T2-Al₂MgC₂ crystals (grey), graphite (black), a 97.7Mg-2.3Al wt.% matrix (light grey) and MgO particles (dark grey).

Table 1. Composition in wt.% (at.%) of the phases formed in 70Mg – 19Al – 11C wt.% samples heat-treated 240 hours at 1000°C

Phase	wt.% (at.%) Mg	wt.% (at.%) Al	wt.% (at.%) C
Matrix	97.7 (97.9)	2.3 (2.1)	-
T2-Al ₂ MgC ₂ exp.	23.9±0.5 (20.2±0.4)	53.2±0.7 (40.5±0.7)	23.0±0.5 (39.3±0.7)
T2-Al ₂ MgC ₂ th.	23.8 (20.0)	52.8 (40.0)	23.5 (40.0)

3.2 Extraction of Al₂MgC₂ single-crystals

If it is assumed that the Al content in the liquid in equilibrium with graphite and T2-Al₂MgC₂ at 1000°C is 2.3 wt.% (2.1 at.%) (cf. 3.1), the fraction of each phase can be found from the overall composition and the composition of each phase at 1000°C. In such case, the liquid in equilibrium with T2-Al₂MgC₂ and graphite at 1000°C accounted for 63 percent of the sample weight. The

weight loss resulting from evaporation was found to be approximately 60 wt.%, which is coherent with the expected loss and suggests that evaporation was complete.

After evaporation, the aspect of the powder compact changed from metallic to friable brown coloured, composed of T2-Al₂MgC₂ single crystals along with graphite, MgO, and Al₄C₃. The Al₄C₃ phase was formed during the evaporation process as it was not found during the SEM analysis performed on the bulk sample after the synthesis. Indeed, as the magnesium evaporates, the liquid becomes richer in aluminium and is able to react with graphite to form Al₄C₃. Optical microscope images of T2-Al₂MgC₂ single-crystals are shown in Fig. 3. The crystals were micrometric and hexagonal platelet-shaped, brownish, transparent and shiny, typically with a smooth surface on one side and a rough surface on the other, and were often found stuck to one another.

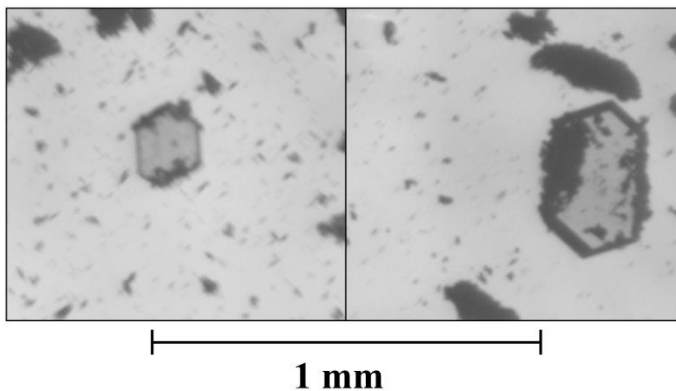


Figure 3. Optical microscope images of T2-Al₂MgC₂ crystals along with graphite at a magnification of 50X. The crystals were plunged in a perfluoropolyether oil to protect them from hydrolysis.

Synthesis and extraction of single crystals of the low-temperature allotropic form of Al₂MgC₂, the so-called T1-Al₂MgC₂ [16], were attempted at 700±4°C for 240 hours. This procedure was unsuccessful as the crystals yielded were too small to be characterized by single-crystal XRD.

3.2 Crystallographic structure of T2-Al₂MgC₂

The T2-Al₂MgC₂ carbide phase synthesized at 1000°C crystallizes in a trigonal structure (space group P-3m1 and Z=1) represented in Fig. 3. The structure and the details of its determination can be found in Table 2. Atom coordinates and thermal displacement parameters can be found in Table 3. Sites were found to be of full occupancy. Distances and angles between atoms can be found in Table 4.

As illustrated in Fig. 4, the crystal structure of T2-Al₂MgC₂ is characterized by alternating layers of Mg occupying the vertices of the trigonal lattice and of Al / C. The Al / C layers are composed of distorted aluminium and carbon tetrahedrons imbricated one in the other. Magnesium atoms are located in a carbon trigonal antiprism. Aluminium atoms are surrounded by a carbon tetrahedron. Carbon atoms are situated inside a polyhedron formed by a trigonal antiprism between three magnesium atoms and a four aluminium atom tetrahedron.

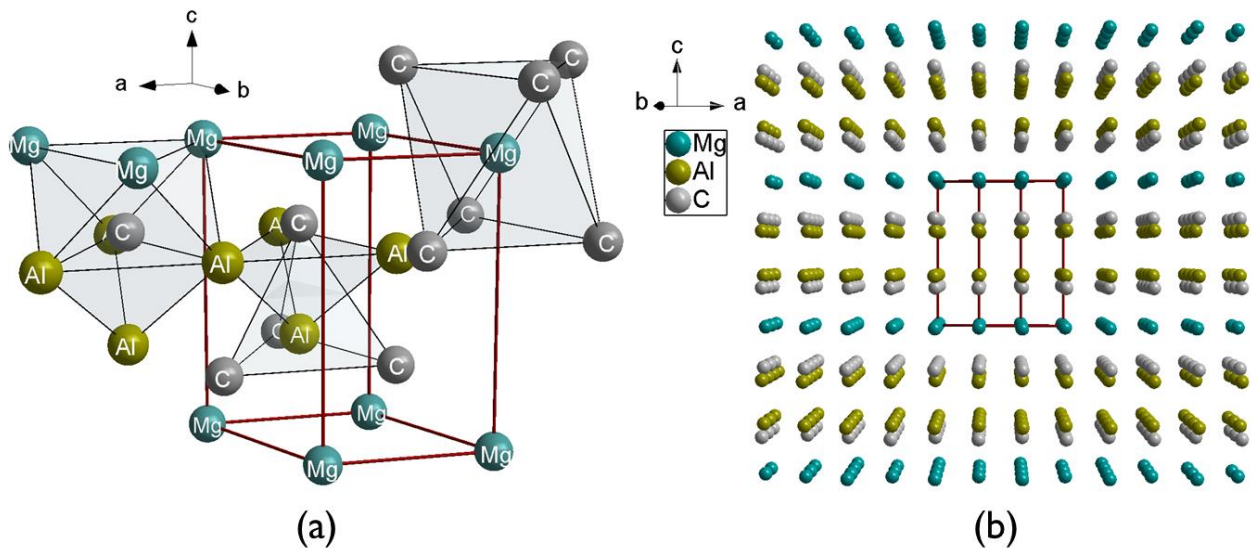


Figure 4. (a) Crystal structure of T2-Al₂MgC₂. Al, C and Mg surroundings as well as Al / C ordering are highlighted. (b) Highlight of the alternating layers of Mg and of Al / C in the structure.

The lattice parameter a of 3.3767 Å, corresponding to the bond length separating Mg atoms, is close to the Mg-Mg distance of 3.2093 Å in the hexagonal close-packed magnesium structure [Str49]. The Al-C bond lengths of 2.0042(11), 2.0045(10), 2.0045(11) and 2.211(4) Å match the Al-C bond lengths observed for the Al₄C₃ phase, viz. 1.89, 1.95 and 2.19 Å [42]. The Mg-C bond length of 2.500(2) Å is slightly longer than the Mg-C bond lengths reported for metastable magnesium carbide phases at atmospheric pressure [43], viz. from 2.21 to 2.46 Å for Mg₂C₃ [44], 2.174(4) Å for MgC₂ [45], and 2.36 Å for Mg₂C recently synthesized by Kurakevych et al. [46]. Therefore, a weak bonding can be expected between the Mg and Al / C layers. As a result, an interesting and challenging perspective would be the delamination of the structure similarly to the formation of MXenes from the MAX phases [47,48] in order to obtain a two-dimensional AlC material.

The lattice parameters found in this work are in very good agreement with those obtained from X-ray powder diffraction in the literature [16,17]. A slight difference is found for the z coordinate of the Al2 and C1 atoms in the structure between this work (respectively 0.6503(2) and 0.2695(6) (cf. Table 3) and the results from Kubus et al. [17] (resp. 0.6525(4) and 0.266(8)) and Bosselet et al. [16] (resp. 0.6226(6) and 0.26531(9)).

Table 2. Structure refinement of T2-Al₂MgC₂

Crystal Shape	Hexagonal Platelet
Crystal Appearance	Transparent and shiny
Crystal Size	0.10x0.09x0.02 mm ²
Crystal System	Trigonal
Space Group	<i>P</i> -3 <i>m</i> 1 (164)
Temperature	150 K
Lattice Parameters	a= 3.3767(11) Å c= 5.807(2) Å
Cell Volume	57.34(5) Å ³
Formula Weight	102.29 g/mol
Z	1
Density, calculated	2.962 g/cm ³
Radiation	MoK _α (λ=0.71073 Å)
hkl range	-5≤h≤5, -5≤k≤5, -9≤l≤9
θ-range	3.45° - 36.06°
Reflections measured	1292
Independent Reflections	139
Reflections I > 2σ(I)	121
Absorption correction	Analytical
R _{int}	0.089
Absorption coefficient	1.127 cm ⁻¹
Transmission min. / max.	0.919 / 0.974
Min / Max residual electron density e ⁻ /Å ³	-0.62 / 0.67
[F ² >2σ(F ²)] / wR(F ²) / S	0.041 / 0.121 / 0.96

Table 3. Coordinates and thermal displacement parameters of T2-Al₂MgC₂ (in Å²)

Atom / Wyckoff position / Site symmetry	x	y	z	U _{eq}	U ₁₁ =U ₂₂	U ₃₃	U ₁₂
Mg1 / 1a / -3m	0	0	0	0.0085	0.0095(6)	0.0065(8)	0.0047(3)
Al2 / 2d / 3m	1/3	2/3	0.6503(2)	0.0059	0.0059(4)	0.0057(6)	0.0030(2)
C1 / 2d / 3m	1/3	2/3	0.2695(6)	0.0053	0.0054(7)	0.0051(12)	0.0027(3)

Table 4. Distances (in Å) and angles (in °) in T2-Al₂MgC₂

Mg1 – C1 ⁱ	2.500(2)	Al2 ^{viii} – Mg1 – Al2 ^{ix}	106.298(10)	C1 ⁱⁱⁱ – Al2 – C1 ^{iv}	114.777(9)
Mg1 – C1 ⁱⁱ	2.500(2)	Al2 ^{viii} – Mg1 – Al2 ^{iv}	179.994(9)	C1 ⁱⁱⁱ – Al2 – C1 ^{vi}	103.44(2)
Al2 – C1 ⁱⁱⁱ	2.0042(11)	Al2 ^{viii} – Mg1 – Al2 ^x	73.706(8)	C1 ^v – Al2 – C1 ^{iv}	114.764(8)
Al2 – C1 ^{iv}	2.0045(11)	Al2 ^{viii} – Mg1 – Al2 ^{xi}	73.706(8)	C1 ^v – Al2 – C1 ^{vi}	103.44(2)
Al2 – C1 ^v	2.0045(10)	Al2 ^v – Mg1 – Al2 ^{ix}	73.706(8)	C1 ^{iv} – Al2 – C1 ^{vi}	103.44(1)
Al2 – C1 ^{vi}	2.211(4)	Al2 ^v – Mg1 – Al2 ^{iv}	73.706(8)	Al2 ⁱⁱⁱ – C1 – Al2 ^{iv}	114.777(9)
C1 – Mg1 ^{vii}	2.500(2)	Al2 ^v – Mg1 – Al2 ^x	106.298(10)	Al2 ⁱⁱⁱ – C1 – Al2 ^v	114.777(9)
Mg1 – Al2 ^{xi}	2.8151(11)	Al2 ^v – Mg1 – Al2 ^{xi}	179.994(9)	Al2 ⁱⁱⁱ – C1 – Al2 ^{vi}	76.56(2)
Mg1 – Al2 ^{vi}	2.8151(11)	Al2 ^{ix} – Mg1 – Al2 ^{iv}	73.703(8)	Al2 ⁱⁱⁱ – C1 – Mg1 ^{vii}	76.482(9)
Mg1 – Al2 ^{viii}	2.8149(10)	Al2 ^{ix} – Mg1 – Al2 ^x	179.993(10)	Al2 ^{iv} – C1 – Al2 ^v	114.764(8)
Mg1 – Al2 ^v	2.8149(11)	Al2 ^{ix} – Mg1 – Al2 ^{xi}	106.292(10)	Al2 ^{iv} – C1 – Al2 ^{vi}	76.565(18)
Mg1 – Al2 ^{ix}	2.8151(11)	Al2 ^{iv} – Mg1 – Al2 ^x	106.292(10)	Al2 ^{iv} – C1 – Mg1 ^{vii}	76.484(9)
Mg1 – Al2 ^{iv}	2.8151(10)	Al2 ^{iv} – Mg1 – Al2 ^{xi}	106.288(11)	Al2 ^v – C1 – Al2 ^{vi}	76.565(18)
C1 ⁱⁱ – Mg1 – C1 ⁱ	95.042(10)	Al2 ^x – Mg1 – Al2 ^x	73.703(8)	Al2 ^v – C1 – Mg1 ^{vii}	154.676(9)
Al2 ^{viii} – Mg1 – Al2 ^v	106.299(11)	C1 ⁱⁱⁱ – Al2 – C1 ^v	114.777(9)	Al2 ^{vi} – C1 – Mg1 ^{vii}	128.758(16)

- (i) x, -1+y, z
(ii) 1+x-y, 1-y, -z
(iii) 1+x-y, 2-y, 1-z
(iv) x-y, 1-y, 1-z
(v) 1+x-y, 1-y, 1-z
(vi) x, y, z
(vii) x, 1+y, z
(viii) x, -1+y, -1+z
(ix) x-y, -y, 1-z
(x) x, y, -1+z
(xi) -1+x, -1+y, -1+z

3.3 Thermodynamic properties of T2-Al₂MgC₂

The calculated lattice parameters and the fully relaxed atomic positions are reproduced in Table 5. The calculated values are in good agreement with the experimental data from single-crystal X-ray diffraction displayed in Tables 2 and 3.

Table 5. Lattice parameters, cell volume and atomic positions of T2-Al₂MgC₂ calculated using the SCAN functional, the VASP code and an energy cutoff of 800 eV

Lattice parameters	a=3.36100 Å c=5.75154 Å			
Cell volume	V= 56.27 Å ³ (0K) V= 56.31 Å ³ (150K) V= 57.48 Å ³ (298K)			
Atom	Symmetry	x	y	z
Mg	1a	0	0	0
Al	2d	1/3	2/3	0.6498
C	2d	1/3	2/3	0.2695

Heat capacities at constant volume and constant pressure were calculated from 0K to 1000K by DFT and were measured at constant pressure by DSC from 300 to 871K. The DSC measurements were performed on the mixture resulting from the extraction of T2-Al₂MgC₂ and corrections had to be applied to take into account the presence of impurities. T2-Al₂MgC₂, graphite, MgO, Al₄C₃, Al and Ta was detected by XRD. It is noteworthy that the hydrolysis of T2-Al₂MgC₂ was prevented during the whole processing as Al₂MgO₄ was not detected. Rietveld analysis was attempted however it could not lead to an accurate determination of phase proportions. Therefore the proportions of some of the impurities can only be known within an interval. The proportion of T2-

Al_2MgC_2 was calculated from the global composition and the composition of each phases as measured by EDS (cf. Section 3.1) and was further supported by microscopy image analysis. The proportion of MgO was estimated between 1 to 6.6 wt.% based on microscopy image analysis. Regarding Al_4C_3 , the phase forms during the evaporation process when the remaining Al react with graphite as discussed in Section 3.2. As the evaporation of Al is negligible at 800°C , the proportion of those Al_4C_3 , Al and graphite phases is therefore linked to the advancement of this reaction and their proportion intervals were selected to be from no reaction to a complete reaction. Finally, the amount of Ta was roughly estimated to be between 1 and 3 wt.%. From the proportion intervals of each impurity an upper and a lower limit of the corrected heat capacity could be obtained resulting in a mean with an uncertainty of $\pm 4.2\%$. This uncertainty adds to the one on the raw heat capacity measurements estimated at $\pm 2.5\%$ [29], and a final combined uncertainty of $\pm 4.9\%$ is determined. The results from DFT and DSC measurements are plotted in Fig. 5. A good agreement is found between experimental and calculations within the uncertainty range.

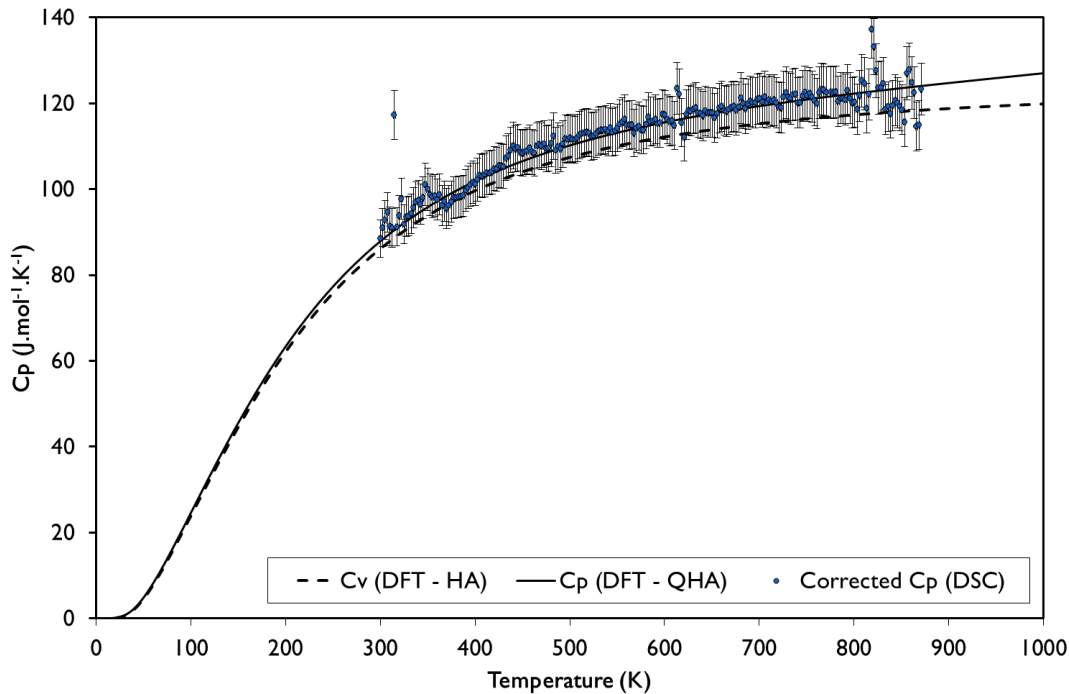


Figure 5. Heat capacity of Al_2MgC_2 as calculated at constant volume using the harmonic approximation (dotted line) and at constant pressure using the quasi-harmonic approximation (solid line) and as measured by DSC (symbols). Corrections were applied on the experimental measurements for the impurities. Because of an insufficient knowledge of the phase proportions, the experimental heat capacity data points plotted are a mean between the upper and lower limit of the corrected results as detailed in the discussion.

The calculated thermodynamic properties of $\text{T2-Al}_2\text{MgC}_2$ are summarized in Table 6. $\text{T2-Al}_2\text{MgC}_2$ is stable with respect to its constituents at 0K and also at room temperature. The entropy of formation was calculated from by integrating the heat capacity data in the quasi-harmonic approximation.

Table 6. Calculated thermodynamic properties of T2-Al₂MgC₂. The heats of formation are referred to elemental Al-fcc, Mg-hcp and C-graphite at the given temperature and the values for Al-fcc and C-graphite were taken from [21]. The heat contents from 0K to 298K of Al-fcc, Mg-hcp and C-graphite used to determine standard heat of formation of T2-Al₂MgC₂ were taken from [31]. A correction of -1.95 kJ/moles of atoms relative to the difference between the ideal C-graphite and true C-graphite was applied to the standard heat of formation of T2-Al₂MgC₂ as described in [21].

$\Delta_f H(0K)$	-20.0 kJ/moles of atoms
$\Delta^{cor} H(0K)$ (with ZPE correction)	-20.9 kJ/moles of atoms
$C_v(298K)$ (DFT – HA)	85.6 J/mol K
$C_p(298K)$ (DFT – QHA)	87.4 J/mol K
$H(298K) - H(0K)$ (from QH approximation)	12.7 kJ/molK
$\Delta_f H(298K)$	-23.6 kJ/moles of atoms
$S^0(298K)$	70.0 J/mol K

3.4 Electronic and lattice dynamic properties of T2-Al₂MgC₂

The calculated electronic density of state (DOS) as well as the band structure of T2-Al₂MgC₂ is presented in Fig.6. An indirect band gap of 1.74 eV was calculated which is close to the value reported for calculations using the GGA functional [19]. It is important to recall, that semi-local DFT calculations tend to underestimate the band gap values and the real experimental value may therefore higher.

The total and partial phonon density of state as well as the phonon band structure is reproduced in Fig. 7. Magnesium essentially contributes to the acoustic branch of the phonon spectrum while carbon is the main contributor to the optical branch. The volumetric thermal expansion β as a

function of temperature T in the quasi-harmonic approximation is presented in Fig. 8. The calculated volume at 298K in the quasi-harmonic approximation is close to the experimental value with a difference below 1%.

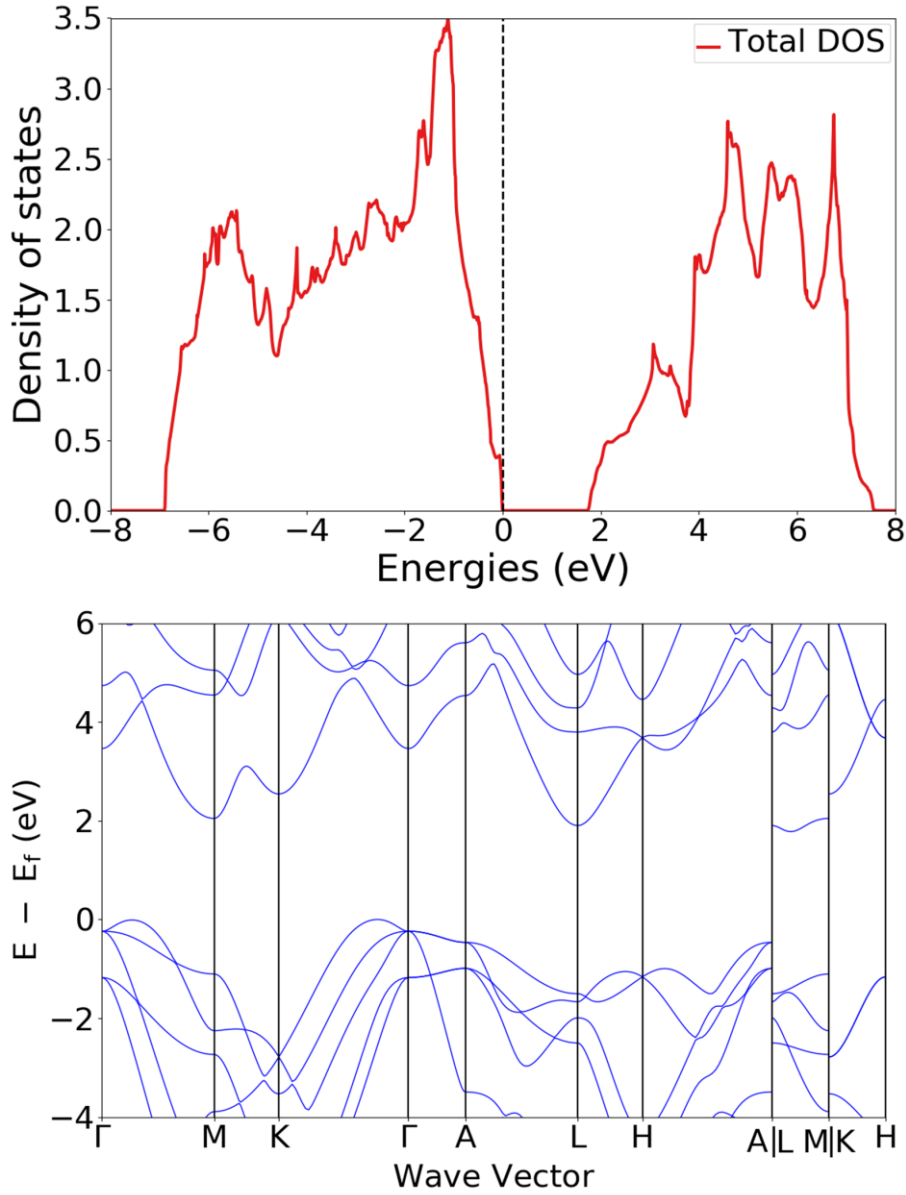


Fig. 6: Calculated total electronic density of states (DOS) and band structure for T2-Al₂MgC₂ from DFT calculations using the SCAN functional.

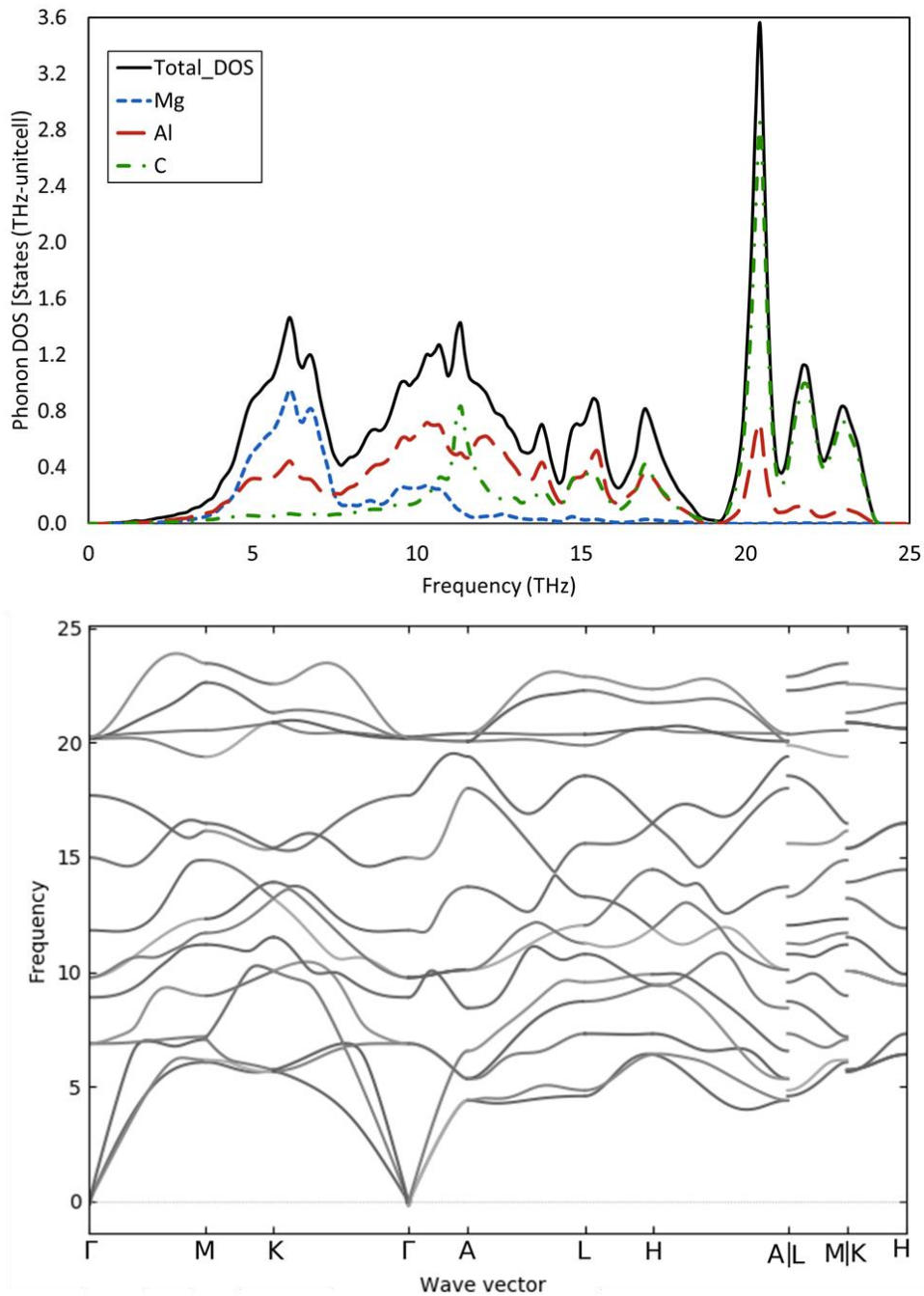


Figure 7. Calculated phonon density of states and phonon band structure for T2-Al₂MgC₂ from DFT calculations using the SCAN functional.

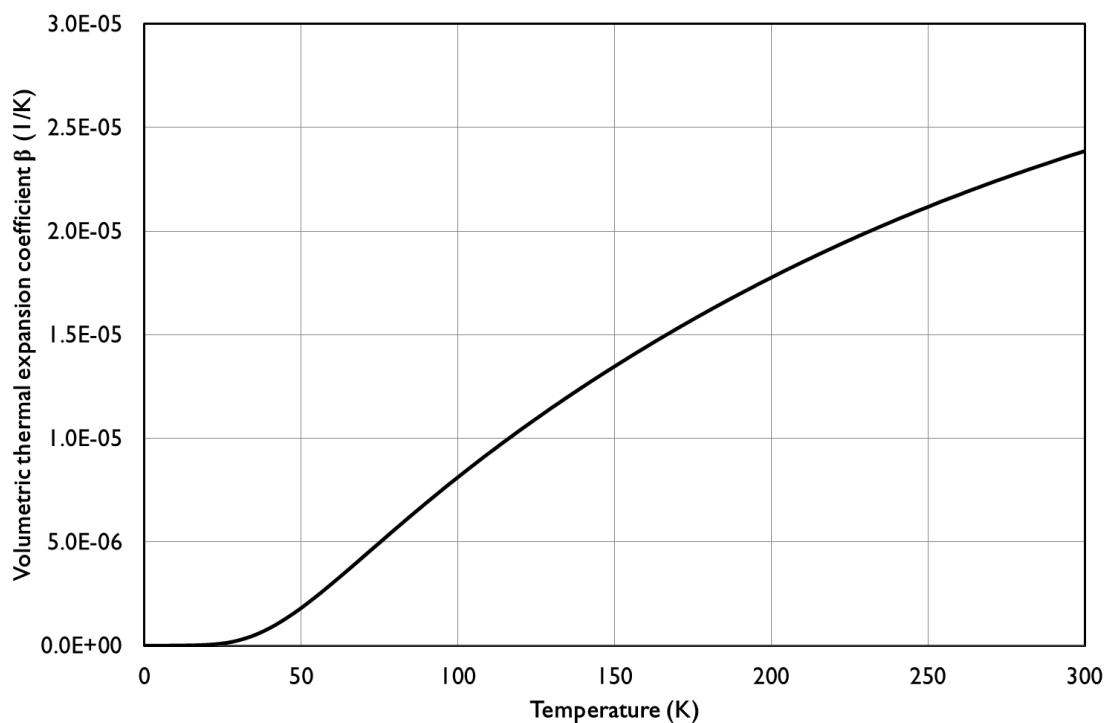


Figure 8. Calculated volumetric thermal expansion coefficient β as a function of temperature T for T2-Al₂MgC₂ in the quasi-harmonic approximation

4. Conclusion

The T2-Al₂MgC₂ phase was synthesized in sealed Ta crucibles. Single-crystals of the allotropic form of Al₂MgC₂, stable above 727°C, were extracted and characterized. The crystal structure of the T2-Al₂MgC₂ was obtained on the basis of single-crystal diffraction and was found to be in good agreement with results in the literature obtained from powder diffraction. Based on the refined structure, DFT calculations were conducted and the enthalpy of formation of T2-Al₂MgC₂ was estimated to be -23.6kJ/moles of atoms at 298K. The heat capacity of T2-Al₂MgC₂ was calculated using the harmonic and quasi-harmonic approximations in good agreement with DSC measurements and the entropy of formation of the phase at 298K was found to be 70.0 J/mol/K. The phonon density of state of the phase is presented and the volumetric thermal expansion

coefficient of T2-Al₂MgC₂ was calculated in the quasi-harmonic approximations. The indirect band gap of the ternary carbide was found to be 1.73 eV. The thermodynamic properties of T2-Al₂MgC₂ investigated in this work are prerequisite for the CALPHAD modeling of the phase. This is the first step toward obtaining a complete thermodynamic database of the Al-C-Mg system, enabling the accelerated development of processes such as the grain refinement of Mg-Al alloys and of Mg-based composites.

This research did not received any specific grant from funding agencies in the public, commercial, or not-for-profit sectors. The authors wish to thank the GDR CNRS n°3584 (TherMatHT) community where fruitful discussions led to collaboration on this project. The assistance of members of the “Centre Technologique des Microstructures, Université Lyon 1” (CTμ, <http://microscopies.univ-lyon1.fr>) for SEM characterizations is gratefully acknowledged. Thanks are also due to Stéphane Martinez (Mechanical Workshop of the University Claude Bernard Lyon 1) and François Cauwet (LMI, Université Claude Bernard Lyon 1) for their help on designing the experimental assembly. The authors are grateful to Catherine Tassin-Arques and Magali Morais (SiMaP, Université Grenoble Alpes) for providing the experimental set-up used to seal the Ta crucibles.

References

- [1] C.J. Bettles, M.A. Gibson, S.M. Zhu, Microstructure and mechanical behaviour of an elevated temperature Mg-rare earth based alloy, *Materials Science and Engineering: A*. 505 (2009) 6–12. doi:10.1016/j.msea.2008.11.004.
- [2] C.H. Caceres, G.E. Mann, J.R. Griffiths, Grain Size Hardening in Mg and Mg-Zn Solid Solutions, *Metallurgical and Materials Transactions A*. 42 (2011) 1950–1959. doi:10.1007/s11661-010-0599-2.
- [3] M. Suresh, A. Srinivasan, K.R. Ravi, U.T.S. Pillai, B.C. Pai, Microstructural refinement and tensile properties enhancement of Mg–3Al alloy using charcoal additions, *Materials Science and Engineering: A*. 528 (2011) 2502–2508. doi:10.1016/j.msea.2010.12.008.
- [4] M. Suresh, A. Srinivasan, U.T.S. Pillai, B.C. Pai, Mechanism for Grain Refinement and Mechanical Properties of AZ91 Mg Alloy by Carbon Inoculation, *Procedia Engineering*. 55 (2013) 93–97. doi:10.1016/j.proeng.2013.03.225.
- [5] J. Du, J. Yang, M. Kuwabara, W. Li, J. Peng, Effects of Carbon and/or Alkaline Earth Elements on Grain Refinement and Tensile Strength of AZ31 Alloy, *MATERIALS TRANSACTIONS*. 49 (2008) 2303–2309. doi:10.2320/matertrans.MRA2008146.
- [6] K.D. Ralston, N. Birbilis, Effect of Grain Size on Corrosion: A Review, *Corrosion*. 66 (2010) 075005-075005–13. doi:10.5006/1.3462912.
- [7] Y.C. Lee, A.K. Dahle, D.H. StJohn, The role of solute in grain refinement of magnesium, *Metallurgical and Materials Transactions A*. 31 (2000) 2895–2906. doi:10.1007/BF02830349.
- [8] Y. Huang, K.U. Kainer, N. Hort, Mechanism of grain refinement of Mg–Al alloys by SiC inoculation, *Scripta Materialia*. 64 (2011) 793–796. doi:10.1016/j.scriptamat.2011.01.005.
- [9] H.-L. Wang, J.-J. Tang, Y.-J. Zhao, J. Du, First-principles study of Mg/Al₂MgC₂ heterogeneous nucleation interfaces, *Applied Surface Science*. 355 (2015) 1091–1097. doi:10.1016/j.apsusc.2015.04.046.
- [10] A. Dey, K.M. Pandey, Magnesium Metal Matrix Composites - A Review, *Reviews on Advanced Materials Science*. 42 (2015) 58–67.
- [11] A. Feldhoff, E. Pippel, J. Woltersdorf, Carbon-fibre reinforced magnesium alloys: nanostructure and chemistry of interlayers and their effect on mechanical properties, *Journal of Microscopy*. 196 (1999) 185–193. doi:10.1046/j.1365-2818.1999.00618.x.
- [12] FactSage FTLite, FactSage Software FTLite database version 7.2 (accessed 03 march 2018), 2018.
- [13] Thermo-Calc TCMG, Thermo-Calc Software TCMG database version 4 (accessed 15 march 2018), 2018.
- [14] CompuTherm PanMg, CompuTherm LLC Pandat Software PanMg2017 DATABASE (accessed 15 march 2018), 2017.
- [15] J.C. Viala, G. Claveyrolas, F. Bosselet, J. Bouix, The chemical behaviour of carbon fibres in magnesium base Mg-Al alloys, *Journal of Materials Science*. 35 (2000) 1813–1825.
- [16] F. Bosselet, B.F. Mentzen, J.C. Viala, M.A. Etoh, J. Bouix, Synthesis, and structure of T₂-Al₂MgC₂, *European Journal of Solid State and Inorganic Chemistry*. 35 (1998) 91–99. doi:10.1016/S0992-4361(98)80017-9.
- [17] M. Kubus, H.-J. Meyer, Convenient Preparation of Ternary Carbidoaluminates - The Example MgAl₂C₂, *European Journal of Inorganic Chemistry*. 2013 (2013) 5450–5453. doi:10.1002/ejic.201300829.

- [18] K.D.M. Harris, M. Tremayne, B.M. Kariuki, Contemporary Advances in the Use of Powder X-Ray Diffraction for Structure Determination, *Angewandte Chemie International Edition*. 40 (2001) 1626–1651. doi:10.1002/1521-3773(20010504)40:9<1626::AID-ANIE16260>3.0.CO;2-7.
- [19] K. Persson, Materials Data on Mg(AlC)₂ (SG:164) by Materials Project, (2014). doi:10.17188/1313297.
- [20] A. Pisch, A. Pasturel, G. Deffrennes, O. Dezellus, G. Mikaelian, P. Benigni, Submitted to *Computational Materials Science*.
- [21] J.L. Kennedy, T.D. Drysdale, D.H. Gregory, Rapid, energy-efficient synthesis of the layered carbide, Al₄C₃, *Green Chemistry*. 17 (2015) 285–290. doi:10.1039/C4GC01277A.
- [22] G. Deffrennes, B. Gardiola, M. Lomello, J. Andrieux, O. Dezellus, R. Schmid-Fetzer, Thermodynamics of Phase Formation in Mg–Al–C Alloys Applied to Grain Refinement, in: D. Orlov, V. Joshi, K.N. Solanki, N.R. Neelameggham (Eds.), *Magnesium Technology 2018*, Springer International Publishing, Cham, 2018: pp. 323–327. doi:10.1007/978-3-319-72332-7_49.
- [23] J. Pouchou, F. Pichoir, Very High Elements x-Ray-Microanalysis - Recent Models of Quantification, *J. Microsc. Spectrosc. Electron*. 11 (1986) 229–250.
- [24] Rigaku Oxford Diffraction, *CrysAlisPro 1.171.38.41*, 2015.
- [25] R.C. Clark, J.S. Reid, The analytical calculation of absorption in multifaceted crystals, *Acta Crystallographica Section A Foundations of Crystallography*. 51 (1995) 887–897. doi:10.1107/S0108767395007367.
- [26] A. Altomare, M.C. Burla, M. Camalli, G.L. Casciarano, C. Giacovazzo, A. Guagliardi, A.G.G. Moliterni, G. Polidori, R. Spagna, *SIR 97*: a new tool for crystal structure determination and refinement, *Journal of Applied Crystallography*. 32 (1999) 115–119. doi:10.1107/S0021889898007717.
- [27] P.W. Betteridge, J.R. Carruthers, R.I. Cooper, K. Prout, D.J. Watkin, *CRYSTALS* version 12: software for guided crystal structure analysis, *Journal of Applied Crystallography*. 36 (2003) 1487–1487. doi:10.1107/S0021889803021800.
- [28] G. Höhne, W. Hemminger, H.-J. Flammersheim, *Differential scanning calorimetry*, Springer, Heidelberg; New York, 2010.
- [29] P. Benigni, G. Mikaelian, R. Pothin, A. Berche, R.M. Ayrat, J.C. Tedenac, P. Jund, J. Rogez, Measurement of the heat capacity of ZnSb by DSC between 300 and 673 K, *Calphad*. 55 (2016) 238–242. doi:10.1016/j.calphad.2016.09.008.
- [30] G.A. Urriano, Standard Reference Material 720 Synthetic Sapphire (α -Al₂O₃), National Bureau of Standards Certificate. (1982).
- [31] M.W. Chase, National Institute of Standards and Technology (U.S.), eds., *NIST-JANAF thermochemical tables*, 4th ed, American Chemical Society ; American Institute of Physics for the National Institute of Standards and Technology, Washington, DC : New York, 1998.
- [32] P. Hohenberg, W. Kohn, Inhomogeneous Electron Gas, *Physical Review*. 136 (1964) B864–B871. doi:10.1103/PhysRev.136.B864.
- [33] W. Kohn, L.J. Sham, Self-Consistent Equations Including Exchange and Correlation Effects, *Physical Review*. 140 (1965) A1133–A1138. doi:10.1103/PhysRev.140.A1133.
- [34] G. Kresse, J. Furthmüller, Efficient iterative schemes for *ab initio* total-energy calculations using a plane-wave basis set, *Physical Review B*. 54 (1996) 11169–11186. doi:10.1103/PhysRevB.54.11169.

- [35] G. Kresse, D. Joubert, From ultrasoft pseudopotentials to the projector augmented-wave method, *Physical Review B*. 59 (1999) 1758–1775. doi:10.1103/PhysRevB.59.1758.
- [36] J. Sun, A. Ruzsinszky, J.P. Perdew, Strongly Constrained and Appropriately Normed Semilocal Density Functional, *Physical Review Letters*. 115 (2015). doi:10.1103/PhysRevLett.115.036402.
- [37] J. Klimeš, D.R. Bowler, A. Michaelides, Chemical accuracy for the van der Waals density functional, *Journal of Physics: Condensed Matter*. 22 (2010) 022201. doi:10.1088/0953-8984/22/2/022201.
- [38] J. Klimeš, D.R. Bowler, A. Michaelides, Van der Waals density functionals applied to solids, *Physical Review B*. 83 (2011). doi:10.1103/PhysRevB.83.195131.
- [39] H.J. Monkhorst, J.D. Pack, Special points for Brillouin-zone integrations, *Physical Review B*. 13 (1976) 5188–5192. doi:10.1103/PhysRevB.13.5188.
- [40] P.E. Blöchl, O. Jepsen, O.K. Andersen, Improved tetrahedron method for Brillouin-zone integrations, *Physical Review B*. 49 (1994) 16223–16233. doi:10.1103/PhysRevB.49.16223.
- [41] A. Togo, I. Tanaka, First principles phonon calculations in materials science, *Scripta Materialia*. 108 (2015) 1–5. doi:10.1016/j.scriptamat.2015.07.021.
- [42] G.A. Jeffrey, V. Wu, The structure of the aluminum carbonitrides. II, *Acta Crystallographica*. 20 (1966) 538–547. doi:10.1107/S0365110X66001208.
- [43] H. Liu, G. Gao, Y. Li, J. Hao, J.S. Tse, Crystal Structures and Chemical Bonding of Magnesium Carbide at High Pressure, *The Journal of Physical Chemistry C*. 119 (2015) 23168–23174. doi:10.1021/acs.jpcc.5b07862.
- [44] H. Fjellvaag, P. Karen, Crystal structure of magnesium sesquicarbide, *Inorganic Chemistry*. 31 (1992) 3260–3263. doi:10.1021/ic00041a018.
- [45] P. Karen, A. Kjekshus, Q. Huang, V.L. Karen, The Crystal Structure of Magnesium Dicarbide, *Journal of Alloys and Compounds*. 282 (1999) 72–75.
- [46] O.O. Kurakevych, T.A. Strobel, D.Y. Kim, G.D. Cody, Synthesis of Mg₂C: A Magnesium Methanide, *Angewandte Chemie International Edition*. 52 (2013) 8930–8933. doi:10.1002/anie.201303463.
- [47] V.M. Hong Ng, H. Huang, K. Zhou, P.S. Lee, W. Que, J.Z. Xu, L.B. Kong, Recent progress in layered transition metal carbides and/or nitrides (MXenes) and their composites: synthesis and applications, *Journal of Materials Chemistry A*. 5 (2017) 3039–3068. doi:10.1039/C6TA06772G.
- [48] O. Mashtalir, M. Naguib, V.N. Mochalin, Y. Dall’Agnese, M. Heon, M.W. Barsoum, Y. Gogotsi, Intercalation and delamination of layered carbides and carbonitrides, *Nature Communications*. 4 (2013). doi:10.1038/ncomms2664.